

Photorefractive asymmetric Fabry–Pérot quantum wells: Transverse-field geometry

K. M. Kwolek,^{a)} M. R. Melloch,^{b)} and D. D. Nolte
Department of Physics, Purdue University, West Lafayette, Indiana 47907-1396

G. A. Brost
Rome Laboratory/OCPA, Griffiss Air Force Base, New York 13441-4515

(Received 9 December 1994; accepted for publication 29 May 1995)

Photorefractive asymmetric Fabry–Pérot quantum-well structures yield significantly enhanced diffraction during four-wave mixing by employing the sensitive amplitude and phase control of multiple-beam interference within the device. We present an $\text{Al}_{0.1}\text{Ga}_{0.9}\text{As}/\text{GaAs}$ photorefractive quantum-well device with a near optimal input diffraction efficiency of 0.36% and an AlAs/GaAs quantum-well device with an output diffraction efficiency of 200%. © 1995 American Institute of Physics.

Photorefractive quantum wells operating in transmission have one of the largest dynamic diffraction efficiencies per interaction length of any known optical materials.^{1–3} However, the device diffraction efficiencies, which are limited by the tradeoff between device absorption and electroabsorption, have not exceeded 3%.⁴ Larger absorption at the exciton transitions produces larger electroabsorption and stronger gratings, but it also reduces the interaction length. This design bottleneck can partly be avoided by operating the photorefractive quantum wells in reflection as asymmetric Fabry–Pérot (ASFP) structures. Quantum-well ASFP modulators have generated the largest contrast ratios in quantum-well structures by utilizing multiple beam interference.⁵ In addition, the multiple beam interference is extremely sensitive to phase, making it possible to operate the ASFP as a phase modulator.⁶ Phase gratings are the most efficient means to diffract light.

In this letter, we present the first experimental demonstration of a photorefractive multiple-quantum-well (MQW) fully asymmetric Fabry–Pérot device. Our device operates in the transverse-field geometry utilizing the Franz–Keldysh effect. Output diffraction efficiencies (defined as the ratio of the first-order diffracted intensity to the transmitted or reflected intensity) as large as 200% have been obtained. This efficiency is significantly larger than previous diffraction efficiencies reported for nearly symmetric Fabry–Pérot devices operating with transverse fields in transmission and reflection⁷ or for non-Fabry–Pérot devices operating with longitudinal fields in transmission.⁴

Peak transverse-field photorefractive ASFP performance relies on the optimization of the electroabsorption properties of the quantum wells, as well as of the Fabry–Pérot. We selected two different structures for our study. In the first structure, we optimized the electroabsorption in the transverse-field geometry for standard temperature growth (STG) quantum wells. A 10% Al fraction in the quantum-well barriers optimizes the sensitivity to the applied field for low fields (the largest absorption change per smallest field

strength), with better diffractive performance than traditional 30% Al-fraction barriers or GaAs thin films.³ This device structure yields absorption changes as large as $\Delta\alpha = 3000 \text{ cm}^{-1}$ for applied fields as small as 8 kV/cm. The design of the STG $\text{Al}_{0.1}\text{Ga}_{0.9}\text{As}/\text{GaAs}$ ASFP was optimized using computer simulations.⁸ A 1.5 μm thick $\text{Al}_{0.1}\text{Ga}_{0.9}\text{As}/\text{GaAs}$ MQW region was chosen to provide the absorption necessary to balance the asymmetric front ($R = 31\%$) and back ($R > 95\%$) mirror reflectivities. The second structure we studied was a low temperature growth (LTG) AlAs barrier MQW. The advantages of LTG AlAs/GaAs quantum wells include higher breakdown field and lower leakage currents. LTG AlAs/GaAs is automatically semi-insulating when annealed.⁹ AlAs barriers yield higher quantum confinement and allow the device to perform at higher fields than $\text{Al}_{0.1}\text{Ga}_{0.9}\text{As}$ barriers.

The photorefractive ASFP devices were grown in a Varian Gen-II molecular beam epitaxy chamber on a GaAs substrate. The STG 10% Al barrier structure, grown at 600 °C, consists of an $\text{Al}_{0.5}\text{Ga}_{0.5}\text{As}$ stop-etch layer beneath a 1.5 μm 100 Å $\text{Al}_{0.1}\text{Ga}_{0.9}\text{As}/75 \text{ Å}$ GaAs MQW region sandwiched between $\text{Al}_{0.1}\text{Ga}_{0.9}\text{As}$ buffer layers used to control the total device thickness. Deep defects were introduced by proton implantation at a double dose of $10^{12}/\text{cm}^2$ at 160 keV and $5 \times 10^{11}/\text{cm}^2$ at 80 keV to make the device semi-insulating throughout the MQW region. The defects provide traps for photorefractive space-charge gratings. The LTG AlAs barrier structure consists of a 2.0 μm 20 Å $\text{AlAs}/100 \text{ Å}$ GaAs MQW region sandwiched between $\text{Al}_{0.1}\text{Ga}_{0.9}\text{As}$ buffers on a $\text{Al}_{0.5}\text{Ga}_{0.5}\text{As}$ stop-etch layer. The stop-etch layer was grown at 600 °C while the MQW region and the buffers were grown at 320 °C. Annealing at 600 °C for 30 s made the material semi-insulating by the formation of As precipitates. The As clusters deplete free carriers from the surrounding material yielding high resistivity. The top surfaces of both structures were coated at Thin Film Lab with a dielectric mirror specially designed for use on semi-insulating material with >95% reflectivity in the 800–900 nm wavelength range centered on the exciton resonances. A room temperature etch in $1\text{NH}_4\text{OH}:19\text{H}_2\text{O}_2$ removed the substrate and HF acid was used to remove any remaining stop-etch material. The HF

^{a)}Electronic mail: karrin@physics.purdue.edu

^{b)}School of electrical engineering.

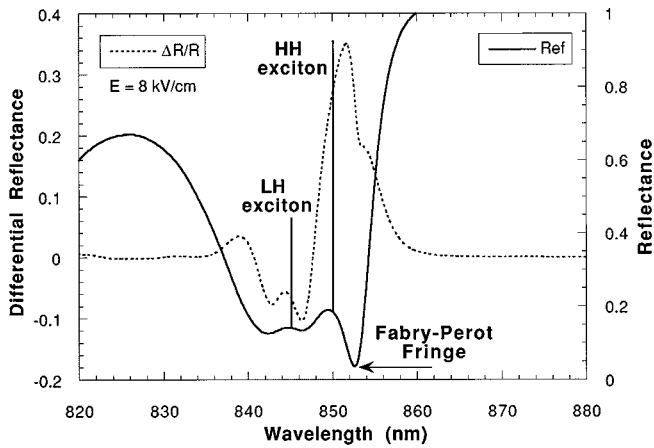


FIG. 1. Zero field reflectance and differential reflectance of the 10% Al barrier device for an 8 kV/cm transverse applied field. The moderate contrast ratio of 35% results from averaging the reflectance over the entire area of the 1 mm \times 2.5 mm device. The light- and heavy-hole exciton transition wavelengths are shown for comparison.

acid soak also maximizes the chance of a good Fabry-Pérot condition because the HF etch rate changes by many orders of magnitude as the aluminum fraction is reduced below 40%.¹⁰ The high-reflectivity rear reflector and careful control of the overall thickness of the device and optical quality of the front and back surfaces increase the chance of a strong and favorably placed Fabry-Pérot resonance. A cold etch (3H₃PO₄:1H₂O₂:5OH₂O) can also be used to remove some of the Al_{0.1}Ga_{0.9}As buffer to tune a Fabry-Pérot fringe to an energy just below that of the heavy hole exciton resonance. After etching, two gold contacts were deposited 1 mm apart on the sample.

The reflectance and differential reflectance for the STG 10% Al barrier device were measured using a monochromator and an 800 V modulated dc field (142 Hz) applied parallel to the quantum wells. The reflectance and differential reflectance are shown in Fig. 1. The Fabry-Pérot minimum reflectance is approximately 4%, averaged over the broad area of the device. The reflection minimum at 852.5 nm lies at the low-energy side of the heavy hole exciton resonance that occurs at 850 nm. The maximum differential reflectance of 35% occurs near the Fabry-Pérot resonance due to the field-induced absorption and index changes. It is important to emphasize that photorefractive quantum-well devices are broad-area devices with active operation areas as large as 1 cm². These devices therefore have more stringent requirements for uniform device thickness over broad areas. As a result, it is difficult to obtain exact Fabry-Pérot cavity resonances over the entire active area, which leads to only moderate contrast ratios of 35% in our devices, averaged over the large device active area.

Nondegenerate four-wave mixing¹ experiments were conducted using two 690 nm diode laser beams to write a diffraction grating with a fringe spacing of 25 μ m. A tunable Ti:sapphire laser was used as a probe beam at an incident angle of 15° with the use of an aperture so that all the probe light fell on the device area and did not overlap the gold contacts. The diffraction efficiency is a strong function of the overall intensity as well as of the intensity ratio of the grating

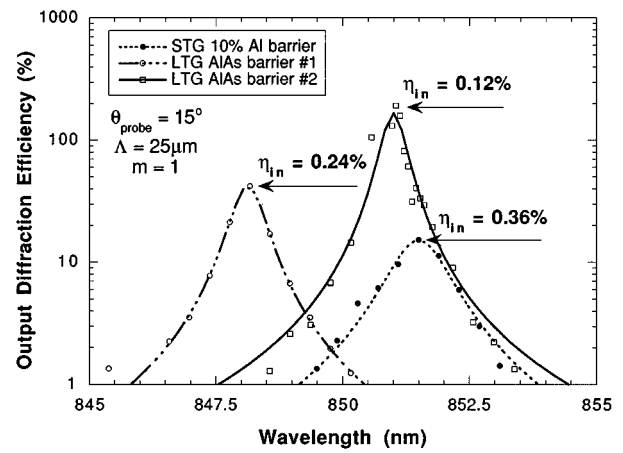


FIG. 2. Output diffraction efficiencies for the MQW ASFPs. The 10% Al barrier device was tested with a modulated dc field of 8 kV/cm at 142 Hz and an approximate total light intensity of 5.0 mW/cm². The two LTG AlAs barrier devices were tested with a modulated dc field of 15 kV/cm at 142 Hz and an approximate total light intensity of 155 mW/cm². Significant enhancement of the diffracted signal is apparent near the Fabry-Pérot resonances for all three devices. Corresponding peak input diffraction efficiencies (η_{in}) for each device are also shown. Lines are to guide the eye.

and probe beams. For the 10% Al barrier device, a probe intensity of 250 μ W/cm² and an approximate grating beam intensity of 4.75 mW/cm² were used. Approximate probe and grating beam intensities of 5 and 150 mW/cm², respectively, were used for the two LTG devices. The zero field reflected and first-order diffraction beams are detected with silicon photodiode detectors through 750 nm long-pass filters. The zero-order beam is mechanically chopped at 142 Hz and detected with a lock-in amplifier while the first order diffraction is detected by modulating the electric field at 142 Hz.

The output diffraction efficiency is defined as the ratio of the diffracted intensity to the transmitted or reflected intensity. In previous reports of photorefractive quantum-well performance, the output diffraction efficiency has been quoted exclusively. However, for many optical systems, it is important to include insertion-loss and device absorption in the diffracted figure of merit. The input diffraction efficiency, defined as the ratio of the diffracted beam to the input beam, is therefore often a more appropriate parameter. The output diffraction efficiencies and the corresponding peak input diffraction efficiencies of the two photorefractive ASFP structures are shown in Fig. 2 as functions of wavelength. The diffraction peak of the 10% Al barrier device is shifted towards the Fabry-Pérot fringe at 852.5 nm. An output diffraction efficiency as large as 15% has been obtained in this device. The diffraction efficiencies from two of the LTG devices are also shown. These two LTG devices differ from each other only in their buffer thickness, and therefore in their Fabry-Pérot fringe position. The output diffraction efficiency reaches nearly 200% for a perfectly balanced cavity in LTG AlAs barrier device No. 2. A different buffer thickness reduces the output diffraction efficiency to 50% in LTG AlAs barrier device No. 1. The corresponding input diffraction efficiency is larger in LTG device No. 1 due to a Fabry-

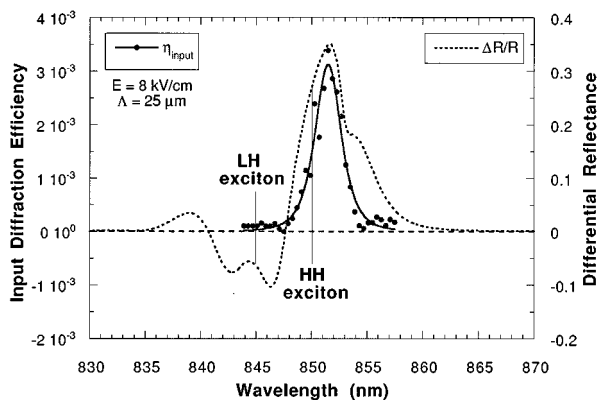


FIG. 3. Input diffraction efficiency, η_{in} , and differential reflectance of the STG 10% Al barrier device demonstrating the influence of the Fabry-Pérot resonance at 852.5 nm on the diffraction. A near optimal η_{in} of 0.36% is achieved for this device geometry.

Pérot resonance closer to the heavy-hole exciton at 844 nm. No significant diffraction is seen at the exciton resonances in these LTG devices. A thicker MQW region and the additional background absorption from the incorporated arsenic precipitates¹¹ lower the input diffraction efficiencies for the LTG devices compared to the STG 10% Al barrier device.

Figure 3 shows the input diffraction efficiency (including all insertion loss and absorption) of the STG 10% Al barrier device superimposed on the differential reflectance. The diffraction maximum occurs between the wavelength of the heavy-hole exciton and the wavelength of the Fabry-Pérot fringe. The maximum input diffraction efficiency from this device is 0.36%. Best transverse-field photorefractive ASFP performance is predicted from computer simulations¹² to yield an input diffraction efficiency of approximately 1%, assuming perfect device growth and fabrication. Therefore, the device demonstrated here has close to the theoretical best performance for this device geometry. Variations in device thickness across the broad area can easily account for the remaining inefficiency. It is important to emphasize that the Fabry-Pérot resonance significantly enhances the diffraction even at the wavelength of the heavy-hole exciton transition. The Fabry-Pérot provides nearly an order of magnitude improvement in the maximum input diffraction efficiency over

non-Fabry-Pérot photorefractive quantum well structures.

In conclusion, we have demonstrated a STG 10% Al barrier transverse-field photorefractive MQW ASFP with a near-optimum input diffraction efficiency of 0.36% and an output diffraction efficiency of 15%. The observed diffraction is significantly enhanced by the Fabry-Pérot resonance. This device design incorporated all important design characteristics for best input diffraction efficiency performance, including optimum barrier Al fraction, high optical surface quality, sufficient absorption to balance the ASFP, and a favorable Fabry-Pérot fringe placement. We also demonstrated an LTG AlAs barrier MQW ASFP with an output diffraction efficiency of nearly 200% but with a lower input diffraction efficiency. Further performance optimization in photorefractive quantum wells may be achieved in longitudinal field geometries using the quantum-confined Stark effect. Computer simulations predict a maximum input diffraction efficiency of 5% for the longitudinal-field geometry.⁸

This work was performed with the support of the United States Air Force Rome Laboratory and the National Science Foundation Award number ECS-9414800. We would also like to acknowledge Thin Film Lab for their design and deposition of the reflective coating used on our devices.

- ¹Q. N. Wang, R. M. Brubaker, D. D. Nolte, and M. R. Melloch, *J. Opt. Soc. Am. B* **9**, 1626 (1992).
- ²D. D. Nolte and M. R. Melloch, *Mater. Res. Bull.* **19**, 44 (1994).
- ³D. D. Nolte and M. R. Melloch, *Photorefractive Quantum Wells and Thin Films, in Photorefractive Effects and Materials*, edited by D. D. Nolte (Kluwer Academic, Dordrecht, 1995), Chap. 7.
- ⁴A. Partovi, A. M. Glass, G. J. Zydzik, H. M. O'Bryan, T. H. Chiu, and W. H. Knox, *Appl. Phys. Lett.* **62**, 3088 (1993).
- ⁵D. S. Gerber, R. Droopad, and G. N. Maracas, *IEEE Photonics Technol. Lett.* **5**, 55 (1993).
- ⁶B. Pezeshki, G. A. Williams, and J. S. J. Harris, *Appl. Phys. Lett.* **60**, 1061 (1992).
- ⁷K. M. Kwolek, M. R. Melloch, and D. D. Nolte, *Appl. Phys. Lett.* **65**, 385 (1994).
- ⁸D. D. Nolte and K. M. Kwolek, *Opt. Commun.* **115**, 606 (1995).
- ⁹M. R. Melloch, J. M. Woodall, E. S. Harmon, D. D. Nolte, N. Otsuka, F. H. Pollak, R. M. Feenstra, and M. A. Lutz, *Annual Review of Materials Science* (Annual Reviews, Palo Alto, CA 1995), Vol. 25.
- ¹⁰E. Yablonovitch, T. Gmitter, J. P. Harbison, and R. H. Bhat, *Appl. Phys. Lett.* **51**, 222 (1987).
- ¹¹D. D. Nolte, *J. Appl. Phys.* **76**, 3740 (1994).
- ¹²D. D. Nolte, *Opt. Lett.* **19**, 819 (1994).